Physica A 674 (2025) 130787

Contents lists available at ScienceDirect

Physica A: Statistical Mechanics and its Applications

journal homepage: www.elsevier.com/locate/physa

Applicability of integral equation theory of molecular liquids to the hydration thermodynamic response to charged particles

Yuki Seno [a,1], Kodai Kanemaru [b,c,1], Shoichi Tanimoto [a,2], Tatsuhiko Miyata [d], Haruyuki Nakano [a], Norio Yoshida [a,c,*]

[a] *Department of Chemistry, Graduate School of Science, Kyushu University, 744 Motooka, Nishi-ku, Fukuoka 819-0395, Japan*
[b] *Fukui Institute for Fundamental Chemistry, Kyoto University, Takano-Nishibiraki-cho 34-4, Sakyo-ku, Kyoto 606-8103, Japan*
[c] *Department of Complex Systems Science, Graduate School of Informatics, Nagoya University, Chikusa-ku, Nagoya 464-8601, Japan*
[d] *Department of Physics, Ehime University, 2-5 Bunkyo-Cho, Matsuyama, Ehime 790-8577, Japan*

ARTICLE INFO

Keywords:
Ion hydration
Dielectric saturation
Reference interaction site model
Molecular Ornstein-Zernike
Molecular dynamics

ABSTRACT

The thermodynamic response of the solvent water to charged particle insertion evaluated by the integral equation theories (IETs) of molecular liquids was assessed. Molecular Ornstein–Zernike (MOZ) and reference interaction site model (RISM) theories were employed as representative theories of IETs, and the results were compared with molecular dynamics (MD) simulations. Both the MOZ and RISM theories showed comparable agreement with MD simulations in the solute charge range of –1.5 to +1, while a large deviation of the hydration free energy was observed at a high magnitude of solute charge. This discrepancy was identified as resulting from excessive solvent distribution in the first hydration shell, which is attributed to the inadequate description of many-body interactions.

1. Introduction

The hydration response of simple ions refers to the intricate interactions that occur when ions dissolve in water—it is a fundamental process in chemistry and biology [1,2]. This phenomenon is driven by the interplay between an ion's electric field and the polar nature of water molecules. When a solute ion is introduced into water, the surrounding water molecules reorganize themselves, orienting their dipoles to counteract the ion's charge. This rearrangement, commonly referred to as hydration or solvation, plays a crucial role in stabilizing the ion in the aqueous medium.

The hydration process is governed by factors such as the ion's charge and size and the dielectric properties of water. Smaller, highly charged ions exhibit stronger electric fields, leading to more extensive hydration shells, comprising one or more layers of water molecules tightly bound to the ion. These hydration shells contribute significantly to the ion's solubility and influence various macroscopic properties of solutions, such as conductivity, viscosity, and ionic strength.

Computational approaches such as molecular dynamics (MD) simulations and integral equation theory (IET) have emerged as

---

[*] Corresponding author at: Department of Complex Systems Science, Graduate School of Informatics, Nagoya University, Chikusa-ku, Nagoya 464-8601, Japan.

E-mail address: noriwo@nagoya-u.jp (N. Yoshida).

[1] These authors contributed equally.

[2] Present address: Department of Biochemistry and Applied Chemistry, National Institute of Technology, Kurume College, 1–1-1 Komorino, Kurume, Japan.

https://doi.org/10.1016/j.physa.2025.130787

powerful tools for probing atomic-level interactions in aqueous solutions, offering insights that complement experimental studies [3–11].

MD simulations provide a dynamic, atomistic view of hydration by tracking the motion of ions and surrounding water molecules over time. This approach allows researchers to analyze hydration shells, diffusion behavior, and the structural reorganization of water molecules in response to ionic electric fields. Additionally, MD simulations can account for the influence of temperature, pressure, and specific ion properties, offering a versatile platform for investigating hydration phenomena under various conditions.

On the other hand, IETs, including approaches such as the reference interaction site model (RISM) or the molecular Ornstein–Zernike (MOZ) theories, provide a statistical mechanical framework for studying solvation [12–25]. By solving equations that describe the spatial distribution of solvent molecules around solutes, IETs offer an efficient method to calculate solvation structures and free energies. IETs complement MD simulations by providing a way to explore larger systems or study long-range interactions.

The hydration response in simple ion hydration is a cornerstone of understanding molecular-level interactions in aqueous solutions. Regarding the dielectric response around ions in water, differing results between MD simulations and IETs have been reported in previous studies.

Kubota and Akiyama analyzed the polarization of water molecules using MD simulations [26]. They examined various solute charges and cell sizes to evaluate finite size effects. The dielectric response of water exhibited strong nonlinearity and was asymmetrical in its response to positive and negative solute charges. As the solute charge increased, a tendency toward linear response was observed. This revealed behavior different from the results obtained using conventional IET, as reported by Kolombet [27].

Kolombet analyzed the dielectric response characteristics in the hydration of monoatomic ions using the RISM theory [27]. The study explored in detail the effects of ion charge and size and of interactions with water molecules on the dielectric response and structure of the hydration shell. Analysis of the nonlinearity and asymmetry of the dielectric response revealed that the response to both positive and negative ions is approximately linear; however, the response coefficient is larger for negative ions than for positive ions. It was shown that the influence of dielectric saturation decreases with increasing ion charge and, for negative ions, additional responses are induced by the hydrogen bonding of water molecules.

In this study, we evaluated the hydration free energy (HFE) of monoatomic ions using RISM and MOZ theories and compared the results with those from MD simulations. Additionally, we decomposed the HFE into its components to examine the major contributors to changes associated with variations in ion charge. Based on these results, we investigated changes in the electrostatic potential and hydration structure, aiming to elucidate the differences between RISM theory, MOZ theory, and MD simulations.

In examining the dielectric response, we briefly describe the reproducibility of the solvent's dielectric constant within the framework of IETs. It is well known that the MOZ theory can accurately reproduce the dielectric constant of a solvent by explicitly treating molecular orientation. In contrast, RISM cannot reproduce the dielectric constant due to its use of interaction sites. Therefore, it is customary to use the DRISM theory proposed by Perkyns and Pettitt to reproduce dielectric constants within RISM [28]. In the present study, the authors also performed calculations using DRISM; however, no qualitative differences were observed in the variation of hydration free energy with respect to changes in ion charge. Thus, to avoid complicating the discussion, DRISM results are not presented in this paper.

2. Computational details

Details of the RISM and MOZ theories and their numerical computational procedure can be found in the literature [5,12–18,20,29,30]. Therefore, only a brief explanation of the RISM and MOZ theories is provided here. The HFE, or, more generally, the solvation free energy, can be expressed by the Kirkwood charging formula. In the framework of RISM theory, it is given by:

$$\Delta\mu = 4\pi\rho\sum_u\sum_v \int_0^1 d\lambda \int_0^\infty r^2 u_{uv}(r) g_{uv}^{\lambda}(r)dr \tag{1}$$

where u_{uv} is the interaction potential between sites u and v, $g_{uv}^{\lambda}(r)$ is a radial distribution function between sites u and v obtained under the charging parameter λ, and ρ is the number density of solvent molecules. The integral by λ appearing on the right-hand side can be analytically evaluated in the framework of the RISM combined with either the hypernetted-chain (HNC) or Kovalenko–Hirata (KH) closure, yielding:

$$\Delta\mu = \frac{4\pi\rho}{\beta}\sum_u\sum_v \int_0^\infty \left[\frac{1}{2}h_{uv}^2(r) - c_{uv}(r) - \frac{1}{2}h_{uv}(r)c_{uv}(r)\right] r^2 dr \tag{2}$$

for the HNC closure and

$$\Delta\mu = \frac{4\pi\rho}{\beta}\sum_u\sum_v \int_0^\infty \left[\frac{1}{2}h_{uv}^2(r)\Theta[-h_{uv}] - c_{uv}(r) - \frac{1}{2}h_{uv}(r)c_{uv}(r)\right] r^2 dr \tag{3}$$

for the KH closure [31–34]. Here, h_{uv} and c_{uv} are the total and direct correlation functions obtained by solving the RISM equation coupled with the corresponding closure, β is the inverse temperature, and Θ is the Heaviside step function. Similar to the case of the RISM, an expression for the HFE can also be derived for MOZ theory coupled with the HNC using the Kirkwood charging formula:

$$\Delta\mu = \frac{4\pi\rho}{\beta}\int_0^\infty \left\{\frac{1}{2}\sum_{mnl\mu\nu}\frac{1}{2l+1}\left\{\left[h_{\mu\nu}^{mnl}(r)\right]^2 - h_{\mu\nu}^{mnl}(r)c_{\mu\nu}^{mnl}(r)\right\} - c_{00}^{000}(r)\right\} r^2 dr \tag{4}$$

where $h_{\mu\nu}^{mnl}$ and $c_{\mu\nu}^{mnl}$ denote the coefficients of multipole expansion of the total and direct correlation functions, respectively [35–37], and m, n, l, μ, and ν denote the order of rotational invariant expansion of the corresponding 6-dimensional correlation functions.

To investigate the solute charge dependency of HFEs, the RISM and MD calculations were performed with varying solute charges from –4.0 to 4.0. The step size of solute charge was 0.2 and 1.0 for the RISM and the MD simulation, respectively. In the case of MOZ, the solute charge was varied from –2.5 to 3.0 in increments of 0.1. This range was chosen because the MOZ calculations did not converge for charges with absolute values greater than this range. The Lennard-Jones (LJ) parameters of the solute were set to be the same as those of oxygen in the SPC/E water model [38]. For solvent water, the SPC/E model was employed. For the RISM calculations, there were 8192 grid points with a spacing of 0.05 Å. The HNC and KH closures were used for the closure relations. 298 K and 0.0333 Å^{-3} for the temperature and number density, respectively. In the RISM calculations, $\sigma_H = 1.0$ Å and $\varepsilon_H = 0.046$ kcal/mol were employed for the hydrogen atom of water. In the MOZ calculations, there were 512 grid points with a spacing of 0.07 Å. The multipole expansion of the solvent was considered up to the fourth order. To run the RISM and MOZ calculations, we used an in-house program code, RISMiCal [30,39,40].

For MD simulations, the thermodynamic integration was performed to evaluate HFEs, as follows:

$$\Delta\mu = \int_0^1 d\lambda_1 \left\langle \frac{\partial U_{uv}(\lambda_1,\lambda_2)}{\partial\lambda_1}\right\rangle_{\text{at}\lambda_2=0} + \int_0^1 d\lambda_2 \left\langle \frac{\partial U_{uv}(\lambda_1,\lambda_2)}{\partial\lambda_2}\right\rangle_{\text{at}\lambda_1=1} \tag{5}$$

where U_{uv} denotes the interaction between the solute and solvent molecules, and $\langle\cdots\rangle$ indicates the ensemble average. We employed an isobaric-isothermal (NPT) ensemble in evaluating these ensemble averages. We introduced two coupling parameters in the MD simulations, λ_1 and λ_2, with which we assumed the following pair potential:

$$u_{\alpha\gamma}^{\text{uv}}(r,\lambda_1,\lambda_2) = 4\lambda_1\varepsilon_{\alpha\gamma}^{\text{uv}}\left[\left(\frac{\left(\sigma_{\alpha\gamma}^{\text{uv}}\right)^2}{r^2+(1-\lambda_1)\delta_{\alpha\gamma}^{\text{uv}}}\right)^6 - \left(\frac{\left(\sigma_{\alpha\gamma}^{\text{uv}}\right)^2}{r^2+(1-\lambda_1)\delta_{\alpha\gamma}^{\text{uv}}}\right)^3\right] + \frac{\lambda_2 q_\alpha q_\gamma}{4\pi\varepsilon_0 r} \tag{6}$$

where ε_0 represents the permittivity of vacuum. In this study, we assumed $\delta_{\alpha\gamma}^{\text{uv}} = 10\ \text{Å}^2$. The indices α and γ denote the atoms in solute and solvent molecules, respectively. The first term of the right-hand side of the pair potential above is the separation-shifted scaling of the LJ potential [41]. The numerical thermodynamic integration was carried out using a step size of 0.2 for each coupling parameter. The simulation box contained 500, 1000, 1500, and 2000 water molecules. The NPT MD simulations were performed with the Nose–Hoover chain thermostat and Andersen barostat for the temperature and pressure control at 298.15 K and 1 atm, respectively [29,42–44]. The bond lengths inside the water molecules were constrained by the "ROLL bonding" method [45]. The periodic boundary condition was applied and the Ewald method was used for handling the Coulomb potential. A time step of 0.5 fs was used, and a 50 ps simulation was performed for each system. The in-house MD simulation code developed by one of the authors (TM) was used for the MD simulations [46–48].

3. Results and discussion

3.1. Assessment of cell size dependency in MD

First, the cell size dependency of HFE evaluated by the MD simulation was assessed. In Table 1, the HFE ($\Delta\mu$) of –4 charged anions for different solvent cell sizes is summarized. Here, $\Delta\Delta\mu$ represents the HFE difference from the value for a system with 500 fewer solvent molecules. As seen, although there is a decrease in HFE with an increase in the number of solvent water molecules, the absolute value of $\Delta\Delta\mu$ gradually decreases. The HFE value is considered to converge, and its convergence value is considered to be substantially higher than the values obtained by IET, as discussed below. Therefore, it is considered that there is no qualitative difference between discussions using any of the systems presented here. In the present study, the system with the lowest number of solvent molecules, # solvent, $N = 500$, which has the lowest computational cost, will thus be used for the following discussion. In addition, Kubota and Akiyama examined the system size dependency and reported that the electrostatic potential exhibits minimal changes for $N \geq 500$

Table 1
Cell size dependency of HFE for –4 charged anion by MD simulation. The HFE and its standard deviation (SD) are denoted as $\Delta\mu$ and SD of $\Delta\mu$, respectively. $\Delta\Delta\mu$ gives the HFE difference from the value for a system with 500 fewer solvent molecules.

# Solvent	$\Delta\mu$[kcal/mol]	SD of $\Delta\mu$[kcal/mol]	$\Delta\Delta\mu$ [kcal/mol]
500	–1415.23	36.16	
1000	–1477.35	35.75	–62.12
1500	–1508.88	35.59	–31.53
2000	–1521.74	36.23	–12.86

[26]. Therefore, $N = 500$ is considered a reasonable choice for a test system.

3.2. Hydration free energy

The solute charge dependency of the HFE evaluated by different computational methods is considered in Fig. 1. The HFE increased negatively as the absolute value of the solute charge increases; in other words, the system becomes more stable. For all methods, the degree of stabilization is greater for anions than for cations. This HFE nature is consistent with the findings of previous studies [26,27]. The results obtained from MD simulations are in good agreement with those from IETs within the range of solute charges from –1.5 to +1. In regions where the absolute value of the solute charge is greater, the IETs tend to overestimate the stabilization of ion hydration compared with MD simulations. The degree of overestimation is greater for anions than for cations. When comparing RISM-KH and RISM-HNC, the degree of overestimation is greater in RISM-HNC. MOZ-HNC exhibits a slightly greater degree of overestimation than RISM-HNC and -KH for cations. For anions, the results of MOZ-HNC appear to agree well with those of RISM; however, calculations were only performed up to a solute charge of –2. Consequently, the behavior for larger negative charges remains unclear.

Before conducting a more detailed analysis, the major components contributing to the changes in HFE were identified. The HFE can be decomposed into the following four components:

$$\Delta\mu = E_{\mathrm{ES}} + E_{\mathrm{LJ}} - T\Delta S_{\mathrm{v}} + E_{\mathrm{Reorg}} \tag{7}$$

where each term on the right-hand side corresponds to the electrostatic interaction, LJ interaction, hydration entropy, and solvent reorganization energy, respectively [49,50]. In the RISM formalism, the electrostatic interaction and LJ interaction terms are given by:

$$E_{\mathrm{ES}} = 4\pi\rho\sum_u\sum_v\int_0^\infty r^2 u_{uv}^{\mathrm{ES}}(r)g_{uv}(r)dr, \tag{8}$$

$$E_{\mathrm{LJ}} = 4\pi\rho\sum_u\sum_v\int_0^\infty r^2 u_{uv}^{\mathrm{LJ}}(r)g_{uv}(r)dr, \tag{9}$$

where $u_{uv}^{\mathrm{ES}}(r)$ and $u_{uv}^{\mathrm{LJ}}(r)$ are the electrostatic and LJ pair interaction potentials. The hydration entropy term is obtained by the numerical differentiation of the HFE respect to temperature:

$$-\Delta S_{\mathrm{v}} = \frac{\Delta\mu(T = 299\mathrm{K}) - \Delta\mu(T = 297\mathrm{K})}{299 - 297}. \tag{10}$$

The solvent reorganization energy is calculated by subtracting these three terms from total HFE, $E_{\mathrm{Reorg}} = \Delta\mu - (E_{\mathrm{ES}} + E_{\mathrm{LJ}} - T\Delta S_{\mathrm{v}})$.

Fig. 2 illustrates the dependence of the HFE and its components on the solute charge evaluated by RISM-HNC. The major component contributing to the stabilization associated with an increase in solute charge is the electrostatic interaction, while the solvent reorganization energy acts to offset this stabilization. The LJ term and the entropy term also act to counterbalance the stabilization, similar to the solvent reorganization energy. However, their contributions are negligible compared with the magnitude of the reorganization energy. The response of the electrostatic interaction to changes in the solute charge will be addressed in later sections.

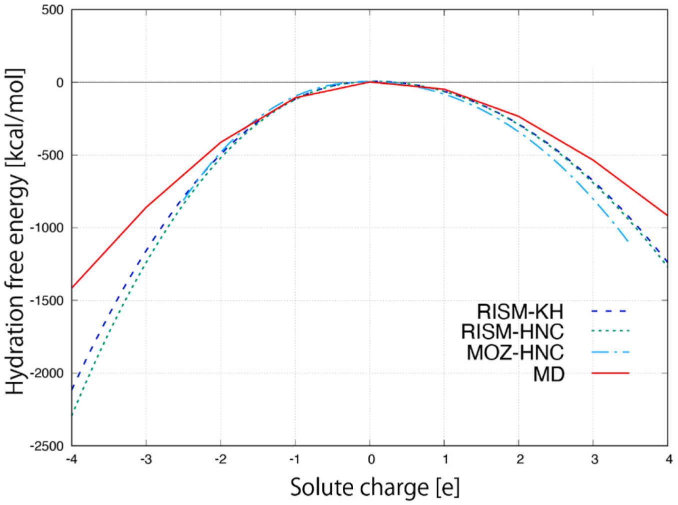

Fig. 1. Solute charge dependency of the HFE evaluated by RISM-KH (blue dashed line), RISM-HNC (green dotted line), MOZ-HNC (cyan dotted/dashed line), and MD (red solid line).

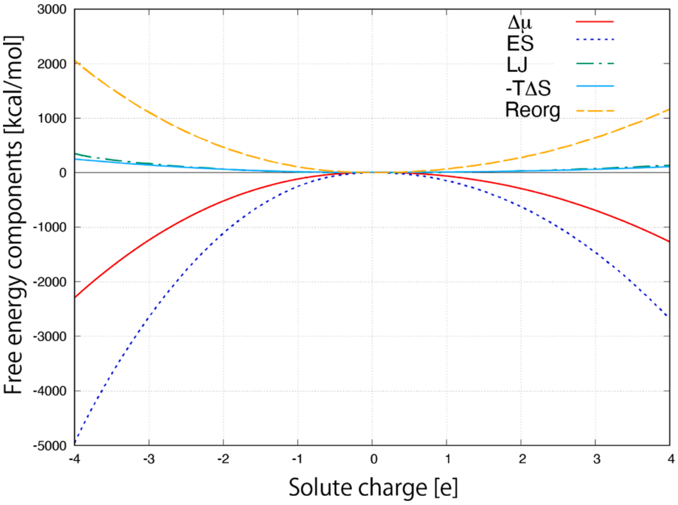

Fig. 2. Components of the HFE. The total HFE ($\Delta\mu$), electrostatic interaction (ES), Lennard-Jones interaction (LJ), hydration entropy ($-T\Delta S$), and solvent reorganization energy (Reorg) are plotted by the following lines, respectively: red solid, blue dotted, green dotted/dashed, cyan solid, and yellow dashed lines.

3.3. Electrostatic potential

The electrostatic potential due to the solvent acting on the solute ion evaluated by RISM-KH, RISM-HNC, MOZ-HNC and MD was plotted against the solute charge. Results are shown in Fig. 3. Here, the MD results are taken from an earlier paper by Kubota and Akiyama [26]. As reported by Kubota and Akiyama, the electrostatic potential varies almost linearly with changes in the solute charge, and the response to anions is greater than to cations. Results from the MD simulations show a change in dependency around –1.5 and +2.0, whereas the IET exhibits linearity with a constant slope across the entire range. The inflection observed in the MD results becomes more evident through the behavior of electrostatic potential fluctuations, as demonstrated in the following analysis.

Fig. 4 plots the fluctuation of the electrostatic potential evaluated by the numerical differentiation of the electrostatic potential shown in Fig. 3. In the MD simulation, electrostatic potential fluctuations increase with the magnitude of the solute charge, reach a maximum value, and then begin to decrease. On the anion side, the fluctuations exhibit greater variation compared with the cation side, reaching a maximum value at –0.5, while the fluctuations on the cation side exhibit a gradual change, reaching a maximum value at +1.0. Interestingly, in the range of solute charges from –0.5 to +1.0, all methods—MD, RISM-KH, RISM-HNC, and MOZ—exhibit qualitatively consistent nonlinear behavior. This consistency is likely due to the ability of each method to adequately reproduce the local interactions between the solute ion and surrounding water molecules. These nonlinear behaviors on the dielectric responses are reported in previous papers using the RISM theory [51,52]. The details of these interactions are discussed later through the analysis of

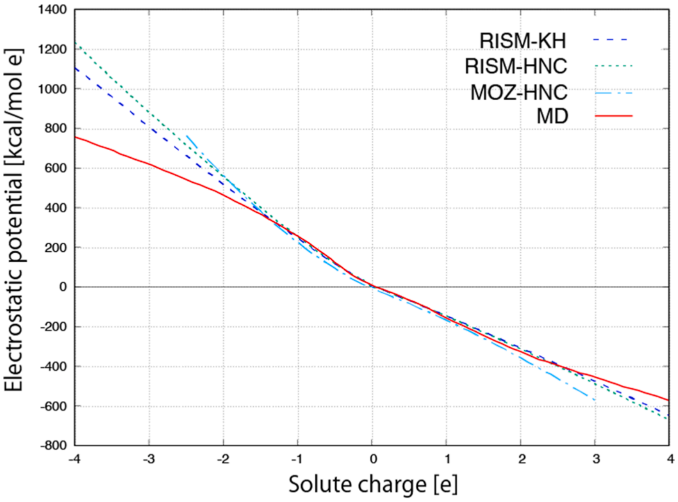

Fig. 3. Electrostatic potential due to the solvent acting on the solute ion. The plots of RISM-KH, RISM-HNC, MOZ-HNC, and MD are blue dashed, green dotted, cyan dotted/dashed, and red solid lines, respectively. The results for MD are taken from the literature Kubota and Akiyama [26].

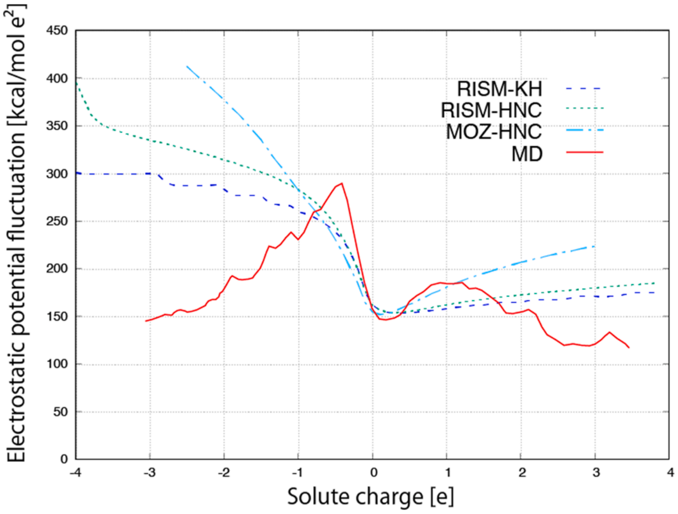

Fig. 4. Fluctuation of electrostatic potential due to the solvent acting on the solute ion. The plots of RISM-KH, RISM-HNC, MOZ-HNC, and MD are blue dashed, green dotted, cyan dotted/dashed, and red solid lines, respectively. The results for MD are taken from the literature Kubota and Akiyama [26].

solvent distribution functions. In contrast, the IETs indicate that electrostatic potential fluctuations increase monotonically but nonlinearly with the magnitude of the solute charge. The variations on the anion side are larger than on the cation side. In the region of low magnitude of solute charge, the results show good agreement with those from MD simulations. Although RISM-KH shows slightly lower values compared with RISM-HNC, the two exhibit qualitatively similar behaviors. MOZ-HNC exhibits greater variations compared with RISM. On the cation side, it consistently yields higher values than RISM. However, on the anion side, in the region where the solute charge is less than –0.5 to –1.0, MOZ-HNC yields lower values than RISM. Beyond this range, with increasing negative charge, the fluctuations in MOZ-HNC increase rapidly. Kolombet and co-workers also reported that IET results show relatively good agreement with MD simulations within a limited range of small charge variations. In the present study, by examining a broader range of ion charges, we were able to identify discrepancies that were not apparent in previous comparisons.

As mentioned in the Introduction, the RISM theory (without employing the Perkyns–Pettitt dielectrically-consistent approach) cannot reproduce the macroscopic dielectric constant. Nevertheless, it exhibits qualitatively similar behavior to MOZ. Although not shown in this paper, we also confirmed that the qualitative behavior remains unchanged when using DRISM. This suggests that the solvent response to solute charge is only weakly influenced by the macroscopic dielectric constant.

In addition, these nonlinear behaviors cannot be readily derived from models like the Born model, highlighting an important advantage of IET and MD approaches in capturing these effects.

3.4. Solvent distribution

As suggested by the results in the previous section, the macroscopic dielectric constant does not significantly affect the dielectric response considered in the present study. Therefore, it is inferred that the microscopic solute–solvent interactions are dominant. This will be examined through the analysis of solvent distributions presented below. In Fig. 5, the radial distribution functions (RDFs) of solvent water around the solute ion are depicted.

The results obtained from the MD simulations are shown in Fig. 5a–d. The solvent water distributions around the solute anions are in Fig. 5a and b for oxygen and hydrogen, respectively. The horizontal axis represents the distance between the ion and the atoms of the solvent water. Due to hydrogen bonding between the anions and water molecules, hydrogen's peak appears at a shorter distance compared with the oxygen peak. Both the hydrogen and oxygen atom distributions shift the first peak toward shorter distances and increase in peak height as the negative charge of the solute increases. Additionally, the second hydrogen peak observed around 3 Å also shifts toward shorter distances while increasing in height. The second oxygen peak exhibits a similar trend. Such behaviors of the distribution functions suggest that the strengthening of hydrogen bonds, driven by the increasing negative charge of the solute, influences even the hydrogen bond network in the second hydration shell.

A similar strengthening of interactions between ions and water molecules is also observed in the case of cations, as shown in Fig. 5c and d. In the case of cations, the negatively charged oxygen atoms orient toward the ion, resulting in the oxygen peak appearing at a shorter distance compared with the hydrogen peak. However, compared with anions, the peak positions appear at longer distances, and their heights are lower. This indicates that the ion–water interaction is weaker for cations than for anions. This observation explains the differences in electrostatic responses discussed for Figs. 3 and 4.

In Fig. 5e–h, the results from RISM-HNC are shown. The changes in the RDF exhibit behavior similar to that observed in the MD simulations; namely, as the magnitude of the charge increases, the peak becomes larger and shifts toward shorter distances. Comparing

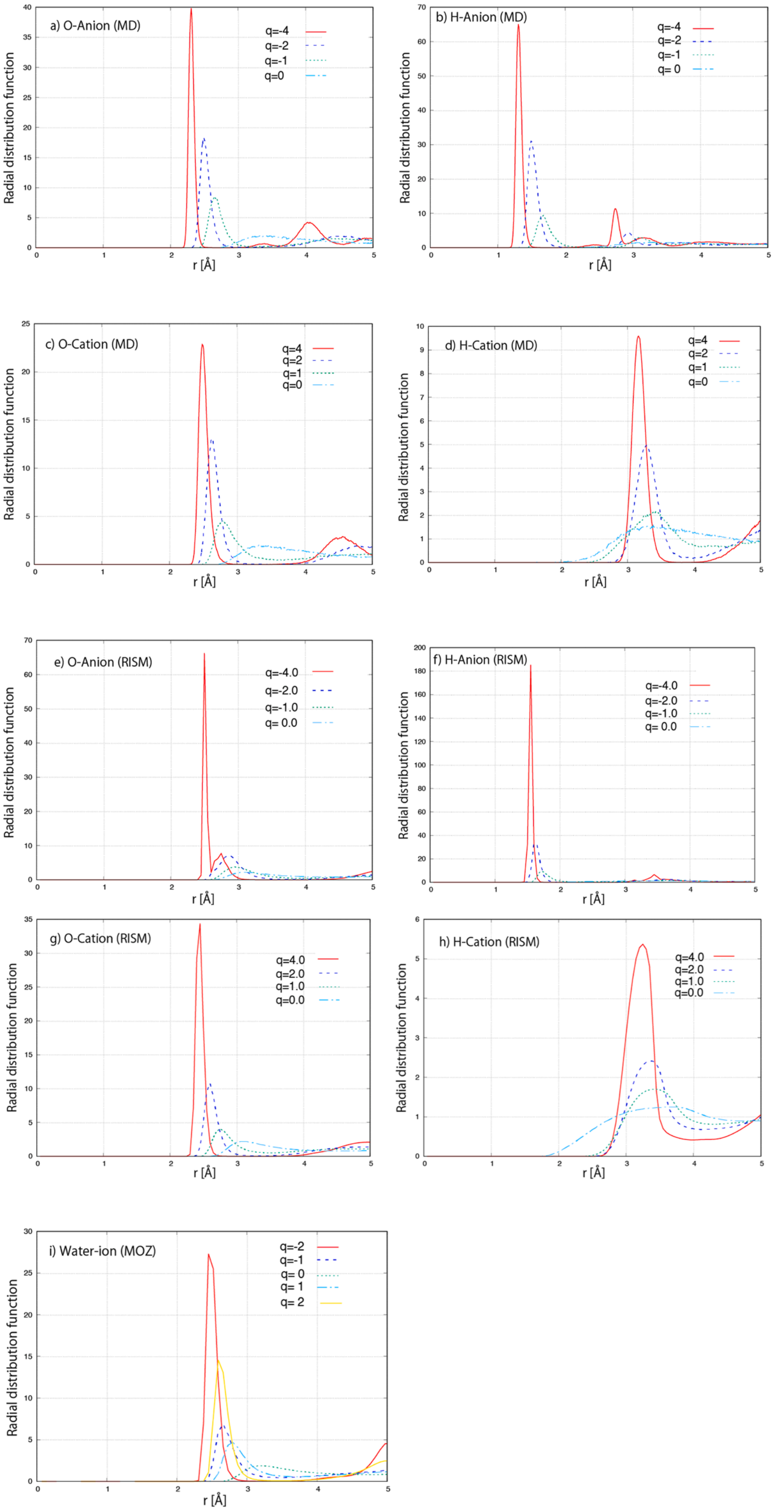

Fig. 5. RDFs of the solvent water around the solute ion. Panels a–d are the RDF plots of the water oxygen-anion, hydrogen-anion, oxygen-cation, and hydrogen-cation evaluated by MD, respectively. Panels e–h are the RDF plots evaluated by RISM-HNC. Panel i is the RDF plot of the center of mass of water molecules and the ions by MOZ-HNC. The legends for the curves are given in the respective panels.

the peak heights with the MD results reveals some interesting features. For anions, when the solute charge is –2 or –1, the hydrogen peak heights are comparable to those obtained from MD simulations. However, for a solute charge of –4, the height of the hydrogen peak is nearly three times higher than the MD results. In the case of oxygen peaks, their heights are approximately half of the MD result for solute charges of –2 and –1, but they exceed the MD peak height when the solute charge is –4. For cations, the oxygen peak heights are comparable to those from MD simulations for solute charges of +2 and +1 but become significantly higher for a solute charge of +4. In contrast, the hydrogen peak heights are lower than in the MD results across all charge states.

The RDF shown in Fig. 5i for MOZ represents the distribution relative to the center of mass of water molecules, which closely corresponds to the oxygen distribution. In the case of a solute charge of –2, the peak height in MOZ is approximately 1.5 times that of the oxygen peak observed in MD simulations. For other cases, the peak heights in MOZ are comparable to those in MD.

Coordination numbers can be calculated from these RDFs. Fig. 6a and b show the running coordination numbers computed from the RDFs of RISM-HNC and MD simulations. Fig. 6a presents the coordination numbers of hydrogen around anions, while Fig. 6b depicts the coordination numbers of oxygen around cations. For neutral solutes and solutes with a charge of –2, the coordination numbers obtained from RISM and MD simulations show good agreement. However, significant discrepancies are observed for solutes with a charge of –4. Specifically, the coordination number in MD simulations remains at about 5, similar to the case of a solute charge of –2, although the peak rises earlier. In contrast, the RISM predicts a dramatic increase in the coordination number within the first hydration shell, reaching approximately 13. The depiction of 13 hydrogen atoms coordinating at a distance of approximately 1.6 Å from the solute appears unphysical.

This result is likely a reflection of the underestimation of intramolecular correlations in the closure relation used in RISM-HNC. In other words, while the orientation of water molecules in the first hydration shell saturates at a solute charge of –2 in MD simulations, such saturation does not occur in the RISM. Similar characteristics are also observed in the coordination numbers of oxygen around cations, as shown in Fig. 6b. For cations, the coordination number of oxygen in MD simulations does not saturate at +2 and shows a slightly higher value at +4 compared with +2. Similarly, the RISM also does not show saturation at +2, with the coordination number increasing further at +4. However, the magnitude of this increase in the RISM is significantly larger than that observed in MD simulations. Such behavior is likely due to the underestimation of excluded volume effects among crowded solvent molecules near highly charged solutes.

4. Conclusions

In this study, we evaluated the validity of the IET in describing the solvent response associated with the insertion of charged particles into an aqueous solvent. As representative frameworks of IETs for molecular liquids, we employed the MOZ and RISM theories. By varying the solute ion charge from –4 to + 4, we examined the HFE, electrostatic potential and its fluctuations, and solvent distributions. For solute ion charges within the range –1.5 to + 1, the descriptions provided by the IETs showed good agreement with MD simulations. However, for solutes with charges exceeding this range, discrepancies with MD results became significant. Analyses based on distribution functions and coordination numbers suggest that the inability of IET to capture electrostatic saturation in the first hydration shell is the primary cause of these discrepancies. This limitation is attributed to an inadequate representation of many-body interactions.

Furthermore, the significant discrepancies between IET and MD observed in this study are likely attributable to the fact that water is an exceptionally unique solvent. As is well known, water serves as a strong source of local electric fields, which is believed to lead to its pronounced nonlinear response. It would be worthwhile to investigate the dielectric response in other polar solvents in future studies [53].

Although discrepancies were observed for solutes with large ion charges, most systems where IET is applied typically involve ions with charges up to ±1. This study demonstrates that IET possesses sufficient accuracy for describing the thermodynamic properties of such systems. Simultaneously, it is important to pay attention when dealing with systems that include divalent ions, such as those found in biomolecular environments. To improve the description of ions with large charges, approaches such as introducing the bridge functions that effectively incorporate many-body interactions or methods based on the inhomogeneous Ornstein–Zernike equation can be considered. We are now investigating the development of such methodologies.

CRediT authorship contribution statement

Seno Yuki: Writing – original draft, Visualization, Methodology, Investigation, Formal analysis, Conceptualization. **Haruyuki Nakano:** Writing – review & editing, Software, Resources. **Norio Yoshida:** Writing – review & editing, Supervision, Software, Resources, Funding acquisition. **Shoichi Tanimoto:** Writing – review & editing, Investigation, Data curation. **Tatsuhiko Miyata:** Writing – review & editing, Supervision, Software, Funding acquisition, Conceptualization. **Kanemaru Kodai:** Writing – review & editing, Investigation, Data curation.

Funding sources

NY is grateful for financial support from the Japan Society for the Promotion of Science (JSPS) KAKENHI (Grant Nos. 19H02677, 22H05089, 22H0173, 24H00282, 24K01434). TM is grateful for financial support from JSPS KAKENHI (Grant No. 23K04666). This work is also supported by the MEXT Program: Data Creation and Utilization-Type Material Research and Development Project (Grant No. JPMXP1122714694), Japan Science and Technology Agency (JST) as part of Adopting Sustainable Partnerships for Innovative

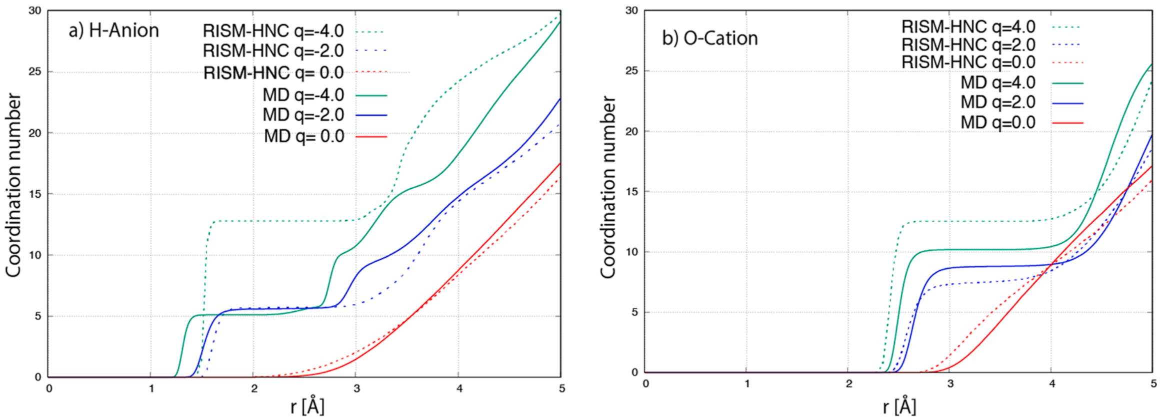

Fig. 6. Running coordination numbers of the solvent water hydrogen (panel a) and oxygen (panel b) around the solute ion evaluated by RISM-HNC and MD simulations. The legends for the curves are given in the respective panels.

Research Ecosystem (ASPIRE), grant number JPMJAP2315, and Toyota Physical and Chemical Research Institute.

Declaration of Competing Interest

The authors declare the following financial interests/personal relationships which may be considered as potential competing interests: Norio Yoshida reports financial support was provided by Japanese Society for Plant Systematics. Norio Yoshida reports financial support was provided by Government of Japan Ministry of Education Culture Sports Science and Technology.

Acknowledgements

Numerical calculations were partially conducted at the Research Center for Computational Science, Institute for Molecular Science, National Institutes of Natural Sciences (Projects 23-IMS-C068, 24-IMS-C066, 23-IMS-C148, and 24-IMS-C146), and use was made of MCRP-S at the Center for Computational Science, University of Tsukuba. This work was supported by MEXT as a “Program for Promoting Research on the Supercomputer Fugaku” (Data-Driven Research Methods Development and Materials Innovation Led by Computational Materials Science, JPMXP1020230327) and use was made of the computational resources of supercomputer Fugaku, provided by the RIKEN Center for Computational Science (Project ID: hp230212, hp240223) and the MEXT Program: Data Creation and Utilization-Type Material Research and Development Project Grant No. JPMXP1122714694.

Data availability

Data will be made available on request.

References

[1] Y. Marcus, Ions in Solution and their Solvation, John Wiley & Sons, 2015.
[2] J. Burgess (Ed.), Ions in Solution: Basic Principles of Chemical Interactions, second ed., Horwood Publishing, Chichester, 1999.
[3] D. Frenkel, B. Smit (Eds.), Understanding Molecular Simulation: From Algorithms to Applications, second ed., Academic Press, San Diego, CA, 2001.
[4] M.P. Allen, D.J. Tildesley, Computer Simulation of Liquids (1987).
[5] F. Hirata (Ed.), Molecular Theory of Solvation, Kluwer, Dordrecht, 2003.
[6] J.P. Hansen, I.R. McDonald (Eds.), Theory of Simple Liquids, 3rd edn., Academic Press, Amsterdam, 2006.
[7] F.O. Raineri, B.C. Perng, H.L. Friedman, Z. Phys. Chem. 204 (1998) 109.
[8] G. Hummer, L.R. Pratt, A.E. Garcia, J. Phys. Chem. 100 (1996) 1206.
[9] R.M. LyndenBell, J.C. Rasaiah, J. Chem. Phys. 107 (1997) 1981.
[10] S. Garde, G. Hummer, M.E. Paulaitis, J. Chem. Phys. 108 (1998) 1552.
[11] S. Rajamani, T. Ghosh, S. Garde, J. Chem. Phys. 120 (2004) 4457.
[12] H. Andersen, D. Chandler, J. Chem. Phys. 57 (1972) 1918.
[13] H. Andersen, D. Chandler, J. Weeks, J. Chem. Phys. 57 (1972) 2626.
[14] D. Chandler, H.C. Andersen, J. Chem. Phys. 57 (1972) 1930.
[15] F. Hirata, P. Rossky, Chem. Phys. Lett. 83 (1981) 329.
[16] L. Blum, J. Chem. Phys. 57 (1972) 1862.
[17] L. Blum, J. Torruella, J. Chem. Phys. 56 (1972) 303.
[18] L. Blum, J. Chem. Phys. 58 (1973) 3295.
[19] F. Garisto, P. Kusalik, G. Patey, J. Chem. Phys. 79 (1983) 6294.
[20] P.H. Fries, G.N. Patey, J. Chem. Phys. 82 (1985) 429.
[21] T. Yamazaki, A. Kovalenko, V.V. Murashov, G.N. Patey, J. Phys. Chem. B 114 (2010) 613.
[22] P. Kusalik, G. Patey, J. Chem. Phys. 86 (1987) 5110.
[23] L. Gendre, R. Ramirez, D. Borgis, Chem. Phys. Lett. 474 (2009) 366.
[24] S. Zhao, R. Ramirez, R. Vuilleumier, D. Borgis, J. Chem. Phys. 134 (2011) 194102.

[25] L. Belloni, D. Borgis, M. Levesque, J. Phys. Chem. Lett. 9 (2018) 1985.
[26] Y. Kubota, R. Akiyama, J. Phys. Chem. Lett. 2 (2011) 1588.
[27] V.A. Kolombet, Russ. J. Gen. Chem. 80 (2010) 1570.
[28] J. Perkyns, B.M. Pettitt, Chem. Phys. Lett. 190 (1992) 626.
[29] H.C. Andersen, J. Chem. Phys. 72 (1980) 2384.
[30] N. Yoshida, S. Kato, J. Chem. Phys. 113 (2000) 4974.
[31] A. Kovalenko, F. Hirata, Chem. Phys. Lett. 290 (1998) 237.
[32] A. Kovalenko, F. Hirata, J. Chem. Phys. 110 (1999) 10095.
[33] A. Kovalenko, F. Hirata, J. Phys. Chem. B 103 (1999) 7942.
[34] S.J. Singer, D. Chandler, Mol. Phys. 55 (1985) 621.
[35] P. Kusalik, G. Patey, J. Chem. Phys. 88 (1988) 7715.
[36] P. Kusalik, G. Patey, J. Chem. Phys. 89 (1988) 5843.
[37] R. Ishizuka, N. Yoshida, J. Chem. Phys. 136 (2012) 114106.
[38] H.J.C. Berendsen, J.R. Grigera, T.P. Straatsma, J. Phys. Chem. 91 (1987) 6269.
[39] N. Yoshida, J. Chem. Info Model 57 (2017) 2646.
[40] Y. Maruyama, N. Yoshida, J. Comput. Chem. 45 (2024) 1470.
[41] M. Zacharias, T.P. Straatsma, J.A. Mccammon, J. Chem. Phys. 100 (1994) 9025.
[42] S. Nosé, J. Chem. Phys. 81 (1984) 511.
[43] S. Nosé, Mol. Phys. 52 (1984) 255.
[44] W.G. Hoover, Phys. Rev. A 31 (1985) 1695.
[45] G.J. Martyna, M.E. Tuckerman, D.J. Tobias, M.L. Klein, Mol. Phys. 87 (1996) 1117.
[46] T. Miyata, Y. Ikuta, F. Hirata, J. Chem. Phys. 133 (2010) 044114.
[47] T. Miyata, Bull. Chem. Soc. Jpn. 90 (2017) 1095.
[48] T. Miyata, S. Murata, M. Sakamoto, Y. Sasaki, AIP Adv. 12 (2022) 035248.
[49] T. Imai, Y. Harano, M. Kinoshita, A. Kovalenko, F. Hirata, J. Chem. Phys. 125 (2006) 024911.
[50] T. Imai, Y. Harano, M. Kinoshita, A. Kovalenko, F. Hirata, J. Chem. Phys. 126 (2007) 225102.
[51] S.H. Chong, F. Hirata, Chem. Phys. Lett. 293 (1998) 119.
[52] R. Akiyama, M. Kinoshita, F. Hirata, Chem. Phys. Lett. 305 (1999) 251.
[53] S.H. Chong, S. Miura, G. Basu, F. Hirata, J. Phys. Chem. 99 (1995) 10526.